Authors' accepted manuscript
Article published in the *Journal of Sound and Vibration*, vol. 459 (27 October 2019)
https://doi.org/10.1016/j.jsv.2019.114873

Numerical and experimental investigations on the acoustic performances of membraned Helmholtz resonators embedded in a porous matrix

Ahmed ABBAD[1,2], Noureddine ATALLA[1], Morvan OUISSE[2], and Olivier DOUTRES[3]

[1] *G.A.U.S., Mechanical Engineering Department, Université de Sherbrooke, 2500 Boulevard de l'Université, Sherbrooke, Quebec J1K 2R1, Canada*

[2] *Univ. Bourgogne Franche-Comté/CNRS/ENSMM/UTBM - FEMTO-ST Institute, 24 rue de l'Épitaphe, 25000 Besançon, France*

[3] *Department of Mechanical Engineering, École de Technologie Supérieure (ÉTS), Montréal, (Qc), Canada, H3C 1K3*

Abstract

Acoustic performances of two concepts based on the integration of an elastic membrane in the front wall of a cavity and Helmholtz resonator embedded in a melamine matrix are studied. Membranes are made of acrylic material, this latter is first characterized with a uniaxial test in order to extract the mechanical properties needed to model the membrane. Analytical, numerical and experimental investigations are performed so as to determine the acoustical potential of the proposed systems in terms of absorption and transmission loss. The contribution to the sound absorption can be positive or negative at the resonator resonances, an analytical model is proposed to highlight the physical phenomena related to these effects. In addition, a multiphysics numerical model combining the acoustic-mechanical interaction has been developed and validated by comparison with the experimental data measured using an impedance tube. The studied concepts could offer significant enhancements of sound transmission loss properties in the low frequencies but also on acoustic absorption in specific frequency bands.

Keywords: Noise reduction, Acoustic absorbers, Helmholtz resonator, Polymer membrane, Absorption and transmission loss efficiency

© 2019. This manuscript version is made available under the CC-BY-NC-ND 4.0 license
http://creativecommons.org/licenses/by-nc-nd/4.0/

1. Introduction

Porous materials are used to reduce noise by absorbing sound energy. As a general rule, thick layers of porous materials are required for low frequency acoustic efficiency [1]. In order to reduce the thickness of sound-packages and to design broadband and efficient acoustic absorbers in the low frequency regime, many configurations have been proposed, among which the use of different resonators, such as coiled slots [2], or sub-wavelength ultra thin acoustic panels based on the use of Helmholtz resonators (HR). A perfect absorption is achieved with a very thin panel in range of frequencies (0-500 Hz) [3]. A HR consists of a neck connected to a cavity which produces a high impedance leading to an attenuation of the acoustic wave. An accurate HR behavior model is essential to achieve the design of high performance device. Historically, the HR behavior has first been assimilated to an equivalent mass-spring mechanical model. Several models have been proposed for the estimation of its resonance frequency. However, the experimental observations yielded to different results as for the calculated frequency, the latter being lower. This is attributed to the oscillation of an additional mass in the resonator neck [4]. Ingard [5] assessed the different corrections to be provided for resonator necks of varied geometries. Selamet [6] studied the influence of the neck shape of the resonator and observed that this had an influence on resonance frequency and transmission loss behavior. A large amount of research is related to the wide use of HRs in a variety of technical applications in different fields of industry [7–10]. For aerospace application, a system used to protect the payloads against noise emission of expandable launch vehicles was proposed by [11]. It is based on the integration of tuned acoustic absorbers (HR with its neck integrated inside the cavity) in foamed plastic mats. This system accomplished high noise reduction in the frequency range up to 90 Hz. Sugie et *al.*[12] investigated the improvement of sound insulation of a double-leaf partition using HRs. The study proposed by Komkin [13] is devoted to analyzing theoretical (based on linear model) and experimental data on sound absorption (using an impedance tube) in a HR as a function of the diameter and length of the resonator neck and its cavity depth, which led to establishing the link between sound absorption of the HR and its geometric parameters. Improving the acoustic properties of sound isolators becomes also possible by combining porous materials with periodically embedded resonators allowing to create effective negative mass density and bulk modulus [14, 15]. Thus, Boutin et *al.* [16] proposed a quasi-analytic

homogenized model of a periodic distribution of HR embedded in a porous matrix. The authors demonstrated the presence of a "co-dynamic" regime resulting from the combination of the porous matrix and the local resonances of the inclusions. The obtained band difference, which can be wide or sharp, is linked to the damping of the resonator and the nature of the flow regime in the matrix where the acoustic wave features are modified. Groby et *al.* [17] studied the effect of integrating a Helmholtz resonator in a foam with different configurations by varying the host material. Integrating the HR leads to a Helmholtz resonance and trapped mode that increases the absorption coefficient. Results show the high impact of the resonator aperture orientation on the material's sound absorption amplitude and bandwidth. Enhancement on the acoustic performances were obtained at low frequencies. Doutres et *al.* [18] investigated theoretically, numerically, and experimentally the acoustic absorption and transmission loss performances of a porous material with HR inclusion. An analytical model based on an extended P-TMM (Parallel transfer matrix method) has been proposed and results validated with measured and FEM (finite elements method) results. The authors pointed out the improvement of the transmission loss at the HR resonance frequency. The absorption coefficient of the foam increases or decreases at the HR resonance, depending on this frequency and the porous material properties. An analysis presented latter in this paper addresses the phenomena governing this effect. The improvement by the HR addition is very important at the resonance frequency of the resonator; outside this zone the efficiency is limited and directly related to the material thickness. In addition, good results in transmission loss of a large curved panel (including 156 HRs) excited under diffuse acoustic field were obtained demonstrating thus, the consistency of the proposed concept. The geometry and the component of a passive resonator are usually fixed for simplicity which limits its acoustic performance to single or very narrow frequency band. Hence and for more specific applications, unconventional resonators systems have emerged. Among others, resonant devices like membrane-type resonators [19] have been proposed as acoustic solution for low frequency control. Vibrational eigenfrequencies are tuned by a small mass on the membrane in order to enhance the acoustic absorption and transmission loss. This has been achieved by varying the membrane and mass properties [20, 21]. Norris and Wickham [22] investigated the effect of the resonator elasticity using a thin elastic spherical shell with a circular aperture subject to plane wave excitation for underwater acoustic applications. The resonance frequency of the obtained Helmholtz resonator can be

shifted down in comparison to the resonance frequency of a rigid resonator. Griffiths et *al.*[23] presented a comparison between absorption measurements and theoretical models of porogranular media made of soft elastomer elastic HRs. It has been demonstrated that the use of a material with a Young's modulus on the order of 1 MPa or less leads to lower the Helmholtz frequency due to the softness of the elastic resonator. Other devices based on flexible-wall acoustic resonators have recently emerged where electroactive polymers (EAPs) made from soft acrylic material have been used to tune a membrane-cavity (dielectric elastomer membrane coupled with a back cavity) resonances [24, 25]. However, the main drawbacks of this type of devices lies in their acoustic performances limited to very narrow frequency bands. Hence, a broadband control can be achieved by combining the effect of a passive material (acoustic foams) for medium and high frequencies and passive inclusions such as elastic membraned resonators for low frequencies (combination of the acoustic and vibrational effect of the membrane). Venegas et.*al* [26] studied numerically and experimentally the wave propagation in permeoelastic system where a fluid-film interaction exists. As a consequence, the geometrical and mechanical properties of the film which is highly viscoelastic seem to play an important role. They strongly affect the effective properties of the system which behaves as an equivalent visco-elastic fluid as well as exhibiting local resonances.

This paper deals with acoustic resonators having a front soft membrane that can be tuned by varying its stretch ratio. Numerical and experimental investigation are performed for a low frequency acoustic resonators with increasing complexity (see Fig.1): (i) rigid Helmholtz resonator, (ii) membrane cavity resonator and (iii) front membrane-cavity Helmholtz resonator. The two membrane-based concepts integrate an acrylic membrane. A numerical model of the acoustic resonators embedded in melamine foam is proposed. The Johnson-Champoux-Allard (JCA) model [27] is used to model the foam acoustical behavior and losses in the resonator's neck [28]. The physical phenomena governing the absorption coefficient behavior at the resonance (positive and negative effect) is discussed through the analysis of the normalized surface impedances of a tuned rigid HR embedded in melamine foam in the case of hard walled termination. When the membrane is integrated into the resonators, the acoustic-mechanical interaction is taken into account in the model in order to obtain a consistent model that properly describes the acoustic performances of the system. Since high deformations are expected in the elastomer membrane, nonlinear elastic models should be considered for

such mechanical behavior. Among others, the Neo-Hookean [29], Mooney-Rivlin [30], Ogden [31] are hyperelastic models that can be used to describe the elastic behavior or the stress-strain constitutive relations of a material from a scalar strain energy function.

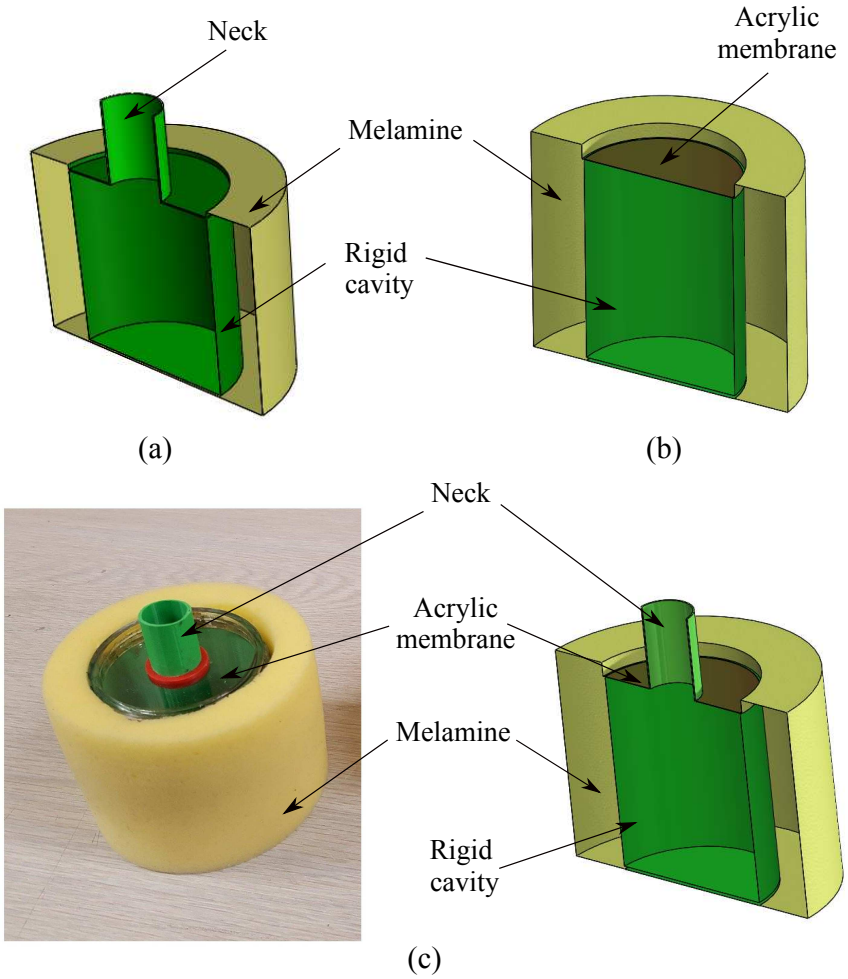

Figure 1: The studied configurations: (a) Rigid Helmholtz resonator in foam (HRF), (b) Membrane-cavity resonator in foam (MCRF), (c) Membrane-cavity Helmholtz resonator in foam (MCHRF): real configuration (left) and 3D schematic (right).

The mechanical properties of the membrane material are identified based on uniaxial tests and results fitted with Ogden hyperelastic model. The ob-

tained parameters are used to simulate the membrane stretch process and therefore compute the in-plane force (for λ=3 and λ=4 stretch ratios). The location of the membrane can be observed in Fig.1 (b, c), which shows the typical design of the membrane-cavity HR system (fully described in Section 2.2). The framework proposed in this paper is particularly appropriate for investigating the acoustic potential of the developed devices. This analysis is performed in term of transmission loss (typically in accordance with aeronautical application), however, understanding the absorption behavior remains essential since practical applications involve double-wall configuration [32]. A discussion using the classical admittance sum method (ASM) [33] is also conducted to better understand the contribution of each element (porous layer and resonator) on the behavior of the composite material.

2. Experimental setup and FEM modeling of membrane-based acoustic resonators

2.1. Description of the devices

Three acoustic devices are studied in this section. The first one is a rigid HR (Fig.1 (a)), the second is a stretched acrylic membrane backed by a cavity (with walls being rigid) of 30 mm radius and 70 mm length (Fig.1 (b)). The third one is based on a HR with a front wall replaced by an acrylic membrane, where a same cavity and neck (added to the membrane) dimensions (listed in Table 1) as in previous cases are used. The cylindrical neck is assembled with the two red rings shown in Fig.1 (c), which are glued to the membrane. Note that the membrane is self-adhesive on both sides which facilitates the attachment of the rings. In both configurations, the filling ratio r is 30% (r is defined as the surface of the resonator relative to that of the foam r=(S_{HR}/S_{foam})). The circular membranes of 30 mm radius used for experiments are prepared using 3M VHB 4910 tapes stretched 3 (and also 4) times in both directions. Once the membranes are stretched, two rings (or supports) of equal size are used to sandwich the membrane thus preventing folding. Both devices are embedded in a 75 mm thick ultralight melamine foam.

Table 1: Dimensions of the studied devices.

	l_{neck} (mm)	r_{neck} (mm)	l_{cavity} (mm)	r_{cavity} (mm)
Cavity	-	-	70	30
HR	30	9	70	30

2.2. Experimental setup for acoustic characterization

The experimental performances of the acoustic devices are investigated using an impedance tube. The experimental setup is shown in Fig.2. It aims at characterizing the acoustic performances of the proposed configurations excited by a plane wave at normal incidence, in terms of absorption coefficient (considering a hard wall configuration) and transmission loss (TL).

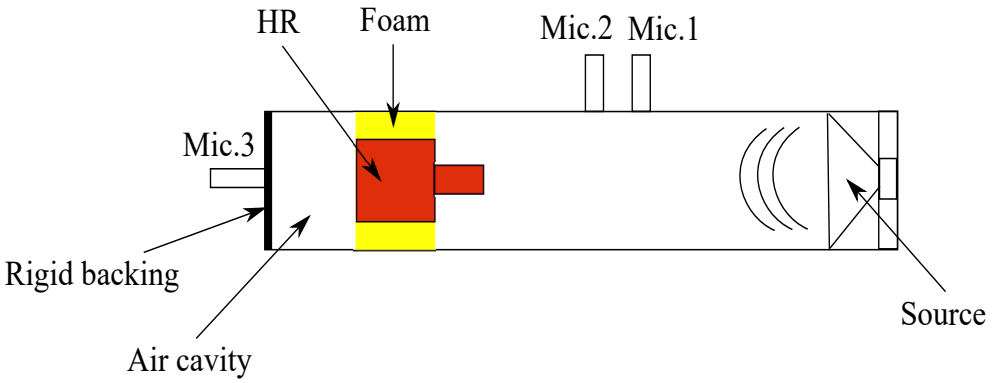

Figure 2: Impedance tube test bench based on the 3 microphones, 2 cavities method used to determine the acoustic performances of the studied devices.

A loudspeaker installed in a 100 mm diameter tube generates a white noise. The three microphones, two cavities (3M2C) method [34] is used to obtain the sample transfer matrix, from which surface impedance, absorption and transmission coefficients are derived. Microphones Mic.1 and Mic.2 are distant of 100 mm. Mic.3 is mounted on a movable hard termination at the end of the tube. Acoustic data acquisitions are operated in the frequency range 100 to 1200 Hz.

2.3. Finite element model of the acoustic devices

This section describes the finite element modeling of the acoustic devices considered in this work.

2.3.1. Membrane vibration modeling

The membrane transverse displacement $w(x, y)$ under harmonic difference pressure load Δp at angular frequency ω is governed by

$$T_0 \bigtriangledown^2 w(x, y) + \omega^2 t \rho_m w(x, y) = \Delta p, \tag{1}$$

where the membrane in-plane force is denoted by T_0, t being the thickness of the membrane material (3M VHB 4910) whose density ρ_m is 960 kg/m^3 and Poisson's ratio is 0.49 [35].
The membrane in-plane force depends on the stretching. It will be estimated using a hyperelastic model described in section 3.1. A $t_0 = 1$ mm thickness material is stretched three (λ=3) and four times (λ=4), the resulting membrane thickness t is reduced to t=$\frac{t_0}{\lambda^2}$ after stretching, leading respectively to 0.11 mm and 0.0625 mm thick membranes (see Section 3). The damping effect is accounted for by using a complex in-plane force T_0^*=$T_0(1 + j\eta)$ with η the damping loss factor of the membrane. A constant damping loss factor of η=0.01 is used in the simulation. Equation (1) is discretized using quadratic Lagrange finite elements.

2.3.2. Acoustic model

A numerical model capable of describing the structural-acoustic coupling is developed in order to predict the acoustic performances of the proposed devices. The acoustic fields inside the tube and resonators cavities are described by Helmholtz's equation

$$\Delta p + k^2 p = 0, \qquad k^2 = \frac{\omega^2}{c_0^2}, \tag{2}$$

where p is the acoustic pressure, k is the wave number and c_0=340 m/s the sound speed in air.

The melamine foam is modeled as an equivalent fluid with a rigid frame based on the Johnson-Champoux-Allard model (JCA) [2]. This model is described by the Helmholtz equation in which the squared sound speed c_0^2

is replaced by $K_{\text{eff}}/\rho_{\text{eff}}$, where K_{eff} and ρ_{eff} are respectively the frequency-dependent effective bulk modulus and effective density. The JCA model is based on five intrinsic experimentally measured properties i.e., the flow resistivity σ, the porosity Φ, the tortuosity α_∞, the viscous Λ and thermal $\Lambda^{'}$ characteristic length. The intrinsic properties given in Table 2 are obtained experimentally from the measurements carried out on the porous materials characterization benches of the Université de Sherbrooke. The visco-thermal losses in the neck of the resonator are considered by using its effective complex and frequency dependent parameters [36, 37] based also on the JCA model: the neck is assimilated to a cylindrical pore [38] with 9 mm radius. The corresponding parameters are provided in Table 2.

Table 2: Johnson-Champoux-Allard model parameters of the ultralight melamine foam; the parameters for the neck are calculated using a cylindrical pore model.

	σ (N s/m^4)	Φ	α_∞	Λ (mm)	$\Lambda^{'}$ (mm)
Foam	8432	0.99	1.02	0.138	0.154
Neck	1.81	1	1	9	9

The numerical model simulates the normal impedance tube measurements in the absorption case wherein the foam is terminated by a hard wall. A unit pressure (1 Pa) is applied on the source side to simulate a plane wave excitation. The 100 mm diameter tube is used on the frequency range 100 to 1200 Hz. The cutoff frequency of the tube is around 1800 Hz. The reflection coefficient R is calculated using the transfer function method. Once the reflection coefficient is determined, the surface impedance [39] is given by

$$Z_s = Z_0 \left(\frac{1+R}{1-R} \right), \qquad Z_0 = \rho_0 c_0, \tag{3}$$

where ρ_0=1.2 kg/m^3 is the air density.

The absorption coefficient represents the ability of a material to absorb the energy of a sound wave. It varies from 0 to 1 and can be computed from the reflection coefficient R as

$$\alpha = 1 - |R|^2. \tag{4}$$

In addition, the sound transmission loss of the devices is also simulated using the FE model. An anechoic termination condition is applied at the end of the tube and the average pressure on a parallel surface (at least one diameter away from the material surface) in downstream $\mathrm{p_{down}}$ is computed.

Transmission loss is determined as

$$\mathrm{TL} = 20 \log_{10} \left(\frac{\mathrm{p_{down}}}{\mathrm{p_{inc}}} \right), \tag{5}$$

where $\mathrm{p_{inc}}$ refers to the 1 Pa amplitude of the incident wave applied on the source side.

3. Mechanical behavior of the hyperelastic membrane

The objective of this section is to identify the model of the membrane for the simulation of the stretching process. The latter will define the mechanical in-plane force in the membrane, which is a key parameter for its tuning when embedded in the acoustic device. In order to describe the mechanical behavior of the elastomer membrane, its material parameters are determined from experiments. The Ogden hyperelastic model is used in this work to describe the behavior of the VHB 4910, which is considered as an incompressible hyperelastic material. The material parameters of the analytical model are identified from uniaxial experimental tests. The selected hyperelastic model is implemented in a finite element model for the simulation of the membrane stretch process which is necessary to obtain the in-plane force of the membrane that controls its vibrating behavior. A brief description of the hyperelastic materials behavior is given in Appendix A for completeness.

3.1. Ogden hyperelastic model

The Ogden model is one of the most widely used hyperelastic material model for predicting the nonlinear stress-strain behavior of rubber-like materials [31]. In this N parameters model, the strain energy density function of the material is given in terms of the three principal stretch ratios. For the uniaxial case, the strain energy density W_s is given by

$$W_s = \sum_{i=1}^{N} \frac{\mu_i}{\alpha_i} (\lambda^{\alpha_i} - 3), \tag{6}$$

corresponding to

$$P_1 = \sum_{i=1}^{N} \mu_i (\lambda^{\alpha_i - 1} - \lambda^{-\frac{\alpha_i}{2} - 1}). \tag{7}$$

where P_1 is the first component of the Piola-Kirchhoff stress tensor, λ the stretch ratio, while μ_i and α_i are empirically determined parameters.

3.2. Material testing method

Uniaxial tests are performed at room temperature (23°C) by stretching the rectangular 3M VHB 4910 material samples to a predefined elongation and measuring the force decrease over time. Tests are performed using a MTS Universal testing machine (Exceed E45). Two 2 mm thick and 25 mm width specimens Sp1 and Sp2 are tested. Sp1 is 131 mm long and Sp2 is 102 mm long. The length of the samples is different in order to obtain the final desired deformation on the testing machine. Sample SP1 is stretched with a strain rate of $\dot{\varepsilon}$=0.5 s^{-1} for an extent deformations up to 400%. A strain rate of $\dot{\varepsilon} = 5\ s^{-1}$ is applied to sample Sp2 up to 500% extent deformation. Table 3 recalls the geometry and the strain rates for samples Sp1 and Sp2.

Sample	Length (mm)	Width (mm)	Thickness (mm)	Strain rate (s^{-1})
Sp1	131	25	2	0.5
Sp2	102	25	2	5

Table 3: Tested specimen properties and strain rates.

At this step, the objective is to identify the hyperelastic model parameters for the simulation of the quasi-static stretching process. Hence, the tests should be performed such that viscoelastic effects are avoided, hence the experimental campaign is restricted to two levels of strain rates, which may be qualified as low strain rates.

Once the material stress-stretch curve is obtained, curve fitting is used to identify the parameters of the hyperelastic material model. Based on the expression of the first Piolla-Kirchoff tensor component P_1 (referred as stress in the following) provided by the model as a function of λ, and given n pairs of measurements (λ_i, P_{1_i}), i= 1...n (the value of n corresponds to the total number of points of the experimental curve), the material parameters are estimated by minimizing the objective function Φ, which expresses

the discrepancy between the experimentally measured and the numerically computed stresses (equation (8)). The mathematical model for the inverse analysis can be expressed as: find parameters (μ_i,α_i) which minimize the function $\Phi(\mu_i, \alpha_i)$ with

$$\Phi = \sum_{i=1}^{n} (P_1(\lambda_i) - P_{1_i})^2. \tag{8}$$

In the next section, experimental results and corresponding fits are presented.

3.3. 3M VHB 4910 characterization results

Fig.3 shows the experimental results in term of stress P_1 versus stretch ratio λ. Lowest strain rate of $\dot{\varepsilon}$=0.5 s^{-1} is applied to sample Sp1. A stretch ratio of λ=4 (which is equivalent to 400% deformation) is imposed (Fig.3; gray curve) with a maximum stress of 105 kPa. For Sp2 (Fig.3; black curve), the strain rate ($\dot{\varepsilon}$=5 s^{-1}) is ten times the one of Sp1. The final stretch is λ=5 (500%) and stress around 180 kPa.

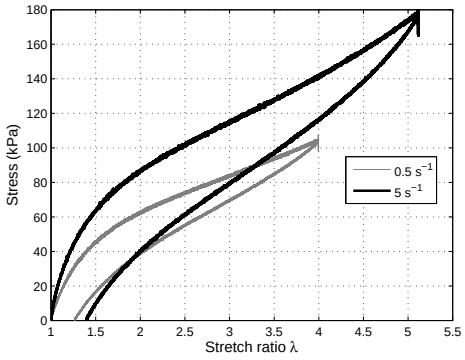

Figure 3: Stress as function of the stretch ratio λ for specimens Sp1 and Sp2.

Only the first part of the experimental data, corresponding to positive stretching is considered for the fitting in order to be in accordance with the effective situation of the membrane in the final resonator.
The Ogden 2nd order model curves are compared to the experimental data in Fig.4(a), (b) and the associated parameters values are listed in Table 4.

Excellent fit with experimental data is observed even for high stretch ratio up to λ=5 (average difference is around 2.3%).

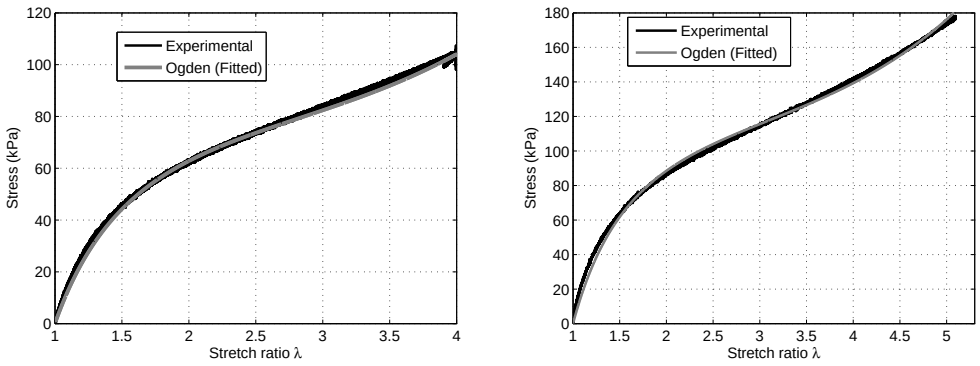

(a) (b)

Figure 4: Experimental and fitted curves for Ogden model: (a) $\dot{\varepsilon} = 0.5\ s^{-1}$, (b) $\dot{\varepsilon} = 5\ s^{-1}$.

The Ogden model appears to be suitable for predicting the VHB behavior since it is able to match experimental results at small and large λ values.

Model	Parameter	$\dot{\varepsilon}$=0.5 s^{-1}	$\dot{\varepsilon}$=5 s^{-1}
Ogden	μ_1(kPa)	104.5	132
	α_1 (-)	0.93	1.02
	μ_2 (kPa)	0.0529	0.0537
	α_2 (-)	5.38	5.27

Table 4: Parameters of 3M VHB 4910 acrylic described by Ogden hyperelastic model for two strain rates $\dot{\varepsilon}$=0.5 s^{-1} and 5 s^{-1}.

In the following, the Ogden model is used in the FEM computations for the simulation of the quasi-static stretching process of the membrane in order to estimate the in-plane force T_0, which is necessary for the description of the vibration movement of the membrane (see Section 2.3.1).

3.4. Membrane stretch FEM modeling

In order to calculate the membrane in-plane force T_0, the parameters listed in Table 4 are used to simulate the membrane stretch process illustrated

in Fig. 5.

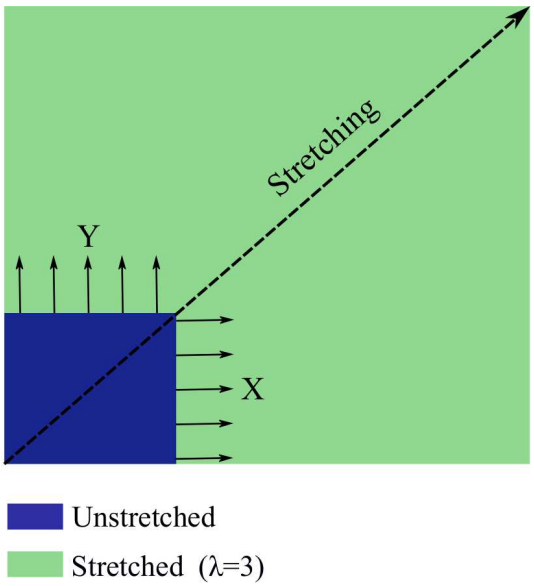

Figure 5: Numerical model of the membrane stretch process: initial case (unstretched) and final case (stretched: λ=3).

The simulation is performed using Abaqus software. The Ogden parameters identified in section 3.3 are used in the FEM computations of the hyperplastic material behavior. The rectangular membrane of 10 mm×100 mm×1 mm membrane is modeled using membrane elements. A displacement of 3 and 4 times the length of the rectangular membrane is imposed in both X and Y directions, given 300 mm and 400 mm length, respectively. A quasi-static study is performed in order to estimate the stress σ of the membrane and the resulted thickness t_0 which allows to calculate the in-plane force T_0=σt_0. Results are listed in Table 5.

Model	Parameter	λ=3	λ=4
Ogden	σ (kPa)	273.2	392.8
	T_0 (N/m)	30.05	24.6

Table 5: Stress σ and membrane in-plane force T_0 obtained from FEM model.

It can be noted that the larger the strain is, the stiffer the VHB tape, as confirmed by the uniaxial curves and the stress values listed in Table 5. The membrane tension is smaller in the case of λ=4 (compared to λ=3) because of the high reduction of the membrane thickness t_0 (0.11 mm and 0.0625 mm, respectively).

4. Results and discussion

This section aims at presenting the performances of the acoustic device in terms of absorption coefficient (considering a hard walled termination) (Equation 4) and transmission loss (Equation 5) obtained through the analytical, experimental and FEM.

4.1. Rigid HR in foam

A rigid HR embedded in a melamine foam (HRF) is first considered (Fig. 1 (a)). The acoustic measurements results are compared to the melamine foam (solid black line) as shown in Fig.6. The HR depicts sound absorption and transmission loss peaks with high amplitude around its resonance frequency (i.e., 298 Hz).

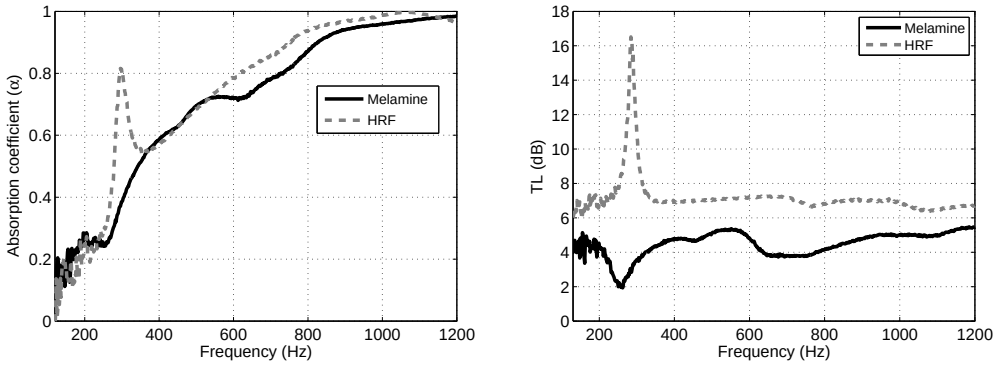

(a) (b)

Figure 6: Experimental sound absorption coefficient (a) and transmission loss (b) results of a rigid Helmholtz resonator compared to melamine foam

These peaks are related to the resonance frequency of the HR embedded in the foam [16, 40]. Outside this resonance, the melamine acoustic transmission loss is improved due to the added mass of the embedded HR. This effect

has been presented through experimental and numerical examples that can be found in the paper by [18]. The authors concluded that it is linked to the resonance frequency of the resonator, the hosting foam size and its acoustic properties but also to the surface ratio of each component. The contribution to the sound absorbing efficiency of the porous material can be positive or negative at the HR resonance.
Hence, we propose here a study based on the analytical expression for the surface admittance of the parallel assembly of a PUC (periodic unit cell) consisting of a rigid HR and the foam weighted by their surface ratios is assessed. The obtained behavior is investigated using the classical admittance sum method (ASM) and the comparison of the resulted normalized surface impedances. The configurations under interest are two rigid HR (tuned at two different frequencies) in parallel with a cavity filled with highly absorbing porous material. The surface admittance Z_s^{PUC} of the resonant PUC is the sum of the surface admittances of the two elements forming the PUC weighted by their surface ratios. It is given by

$$\frac{1}{Z_s^{\mathrm{PUC}}} = \frac{r}{Z_s^{\mathrm{HR}}} + \frac{1-r}{Z_s^{\mathrm{M}}}, \tag{9}$$

where Z_s^{HR} and Z_s^{M} are the surface admittances of the rigid HR and the melamine foam, respectively. Detailed analytical expressions for the HR and the foam surface impedances Z_s^{HR} can be found in [18].

Equation (9) is now written in terms of the real and imaginary parts of the surface impedance of the two components $Z_s^{\mathrm{HR}} = X + jY$ and $Z_s^{\mathrm{M}} = P + jQ$ such as:

$$\mathrm{Re}(Z_s^{PUC}) = \frac{X|Z_s^{\mathrm{M}}|^2/(1-r) + P|Z_s^{\mathrm{HR}}|^2/r}{r|Z_s^{\mathrm{M}}|^2/(1-r) + (1-r)|Z_s^{\mathrm{HR}}|^2/r + 2(PX+QY)} \tag{10}$$

$$\mathrm{Im}(Z_s^{PUC}) = \frac{Y|Z_s^{\mathrm{M}}|^2/(1-r) + Q|Z_s^{\mathrm{HR}}|^2/r}{r|Z_s^{\mathrm{M}}|^2/(1-r) + (1-r)|Z_s^{\mathrm{HR}}|^2/r + 2(PX+QY)} \tag{11}$$

For extreme values of r, ($r \to 0$ and $r \to 1$), the behavior of the patchwork is fully governed by one of the two elements. However, for intermediary values of r, the asymptotic behavior of equations (10) and (11) can be analyzed to better understand the influence of the HR. Two different configurations are

presented in Fig.7 to illustrate the influence of the HR tuning frequency f_0 when a HR is placed in a highly absorbing media (see properties in Table 2). The HR cavity thickness is d=7cm and its surface ratio is r=60%. For each configuration, Fig.7 presents the sound absorption coefficient (see first line in Fig.7) and the normalized surface impedance (second line in Fig.7) of the parallel assembly and of the two elements weighted by their respective surface ratio. In the first configuration, the HR is tuned to 190 Hz and creates a sound absorption peak (see Fig.7 (a)), whereas in the second configuration the HR is tuned to 435 Hz and causes a sound absorption dip (see Fig.7 (c)).

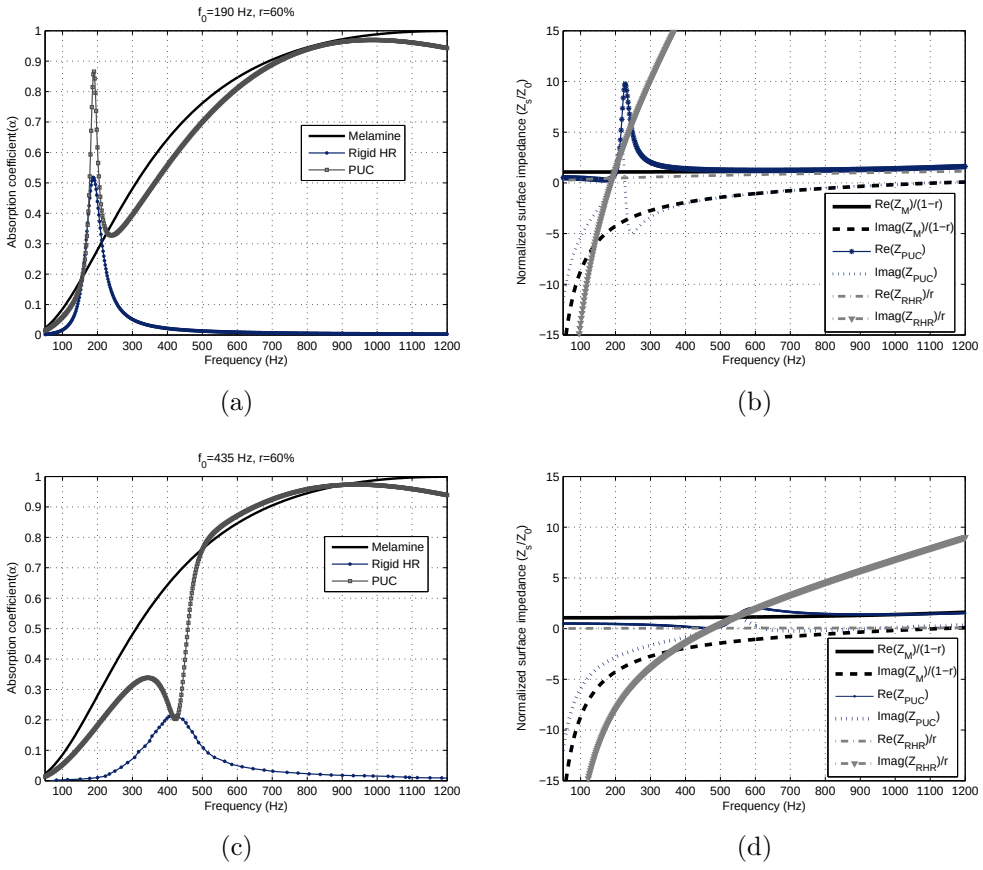

Figure 7: Influence of the HR tuning frequency on the sound absorption efficiency of a highly absorbing material. Simulations carried out using the ASM formulation. a, c) sound absorption coefficient; b, d) normalized surface impedance. first line) HR tuned at 190 Hz; second line) HR tuned at 470 Hz.

For $f<f_0$ and $f>f_0$ the imaginary part of the HR, Y, is much more important compared with both the real part and the imaginary part of the foam material (see Fig.7 (b) and (d)). Equations (10) and (11) thus show that in this case, $(Z_s^{\mathrm{PUC}})_{f<f_0,f>f_0} \rightarrow (P+jQ)/(1-r)=Z_s^{\mathrm{M}}/(1-r)$ which is equivalent to say that the surface impedance of the resonant PUC is controlled by the porous element. Fig.7 confirms this asymptotic behavior for frequencies above and below f_0 where the acoustic behavior of the parallel assembly is very similar to the one of the porous material weighted by the surface ratio (1-r).

At $f=f_0$ the imaginary part Y of the HR impedance is null. Moreover, since the resistance and more importantly the reactance of the foam are much higher than the resistance X of the HR, one has $X|Z_s^{\mathrm{M}}|^2>>|X|^2$. This inequality still holds for intermediary surface ratio r and $X|Z_s^{\mathrm{M}}|^2/(1-r)>>|X|^2/r$. In this case, equations (10) and (11) show that $\mathrm{Re}(Z_s^{\mathrm{PUC}})\rightarrow X/r$ and $\mathrm{Im}(Z_s^{\mathrm{PUC}})\rightarrow 0$: the surface impedance of the resonant PUC is controlled by the resonator.
At the HR resonance frequency of both configurations, Fig.7 (b, d) show that the real part of the total surface impedance $\mathrm{Re}(Z_s^{\mathrm{PUC}})$ decreases to reach the one of the HR and the imaginary part $\mathrm{Im}(Z_s^{\mathrm{PUC}})$ increases to cross the zero axis. Since the resonator controls the impedance around the resonance, the absorption of the assembly is highly corrected with (tends towards) the one of the HR alone. In the first configuration, the resonance arises in a frequency region where the absorption of the foam is low (Fig.7 (a)) because of the large reactance (Fig.7 (b)). In consequence, the addition of the HR results in a peak of absorption. On the contrary, in the second configuration, the resonance is in region where the absorption of the foam is much higher than the one of the HR (Fig.7 (c)). The addition of the resonator results in a decrease of the resistance (Fig.7 (d)) and therefore loss of absorption.

4.2. Membrane-cavity resonator in a foam

Sound absorption and transmission loss of a membrane-cavity embedded in a melamine foam (MCRF) with two stretch ratios are considered. The tested device is shown in Fig.1 (b).
Fig.8 and 9 show the comparison between measured and simulated absorption coefficient and transmission loss of the membrane-cavity for the two cases of interest, ie. λ=3 and λ=4. The figures also show a reference result

corresponding to a melamine sample occupying the full volume (ie. without resonator). The melamine curve obtained from absorption measurement (black solid line) shows a maximum absorption peak of 30% at 200 Hz and a resonance at 250 Hz attributed to the mechanical resonance of the melamine matrix (Biot frequency). Thus, the 1/4 wavelength of the foam is observed and results in dips in both the absorption and transmission loss curves. This resonance frequency may be approached by considering the properties of the foam frame [41]. Above this resonance, a transmission loss of 5 dB is obtained in the frequency range 200 to 1200 Hz corresponding to the foam contribution. This is easily captured by a rigid frame model of the foam.

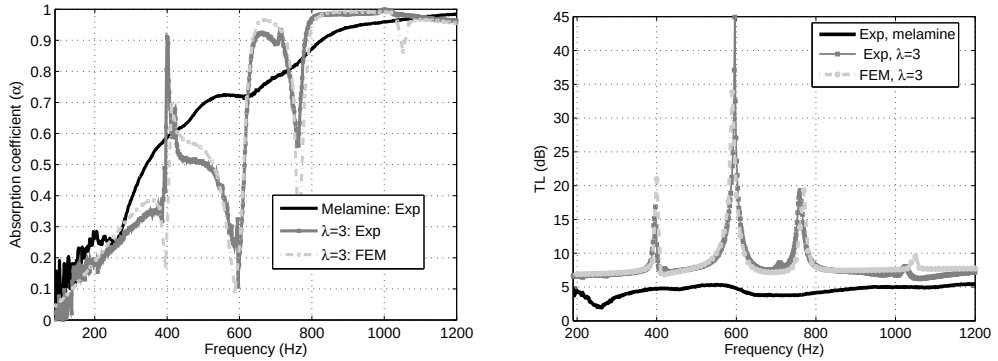

(a) (b)

Figure 8: Measurements and numerical results comparison of the membrane-cavity for λ=3 compared to the melamine foam: (a) Absorption coefficient, (b) Transmission loss.

It can be seen that for the two considered stretch ratios values, the predicted and measured absorption coefficient and transmission loss match well. However this good correlation could be obtained only after an updating of the membrane in-plane force T_0. The membrane in-plane forces T_0 listed in Table 5 provides from the simulated stretching process are T_0=30.05 N/m for λ=3 and T_0=24.55 N/m for λ=4. These values turn out to be highly sensitive to the strain rate during the experimental stretch, which results in uncertainties on the T_0 values. To overcome this issue, an identification process (which consists in finding T_0 that minimizes the $\Phi(T_0)$ function based on Least Mean Square algorithm (equation (8))), is used to obtain the effective in-plane force which better fits the experiments. The corresponding values

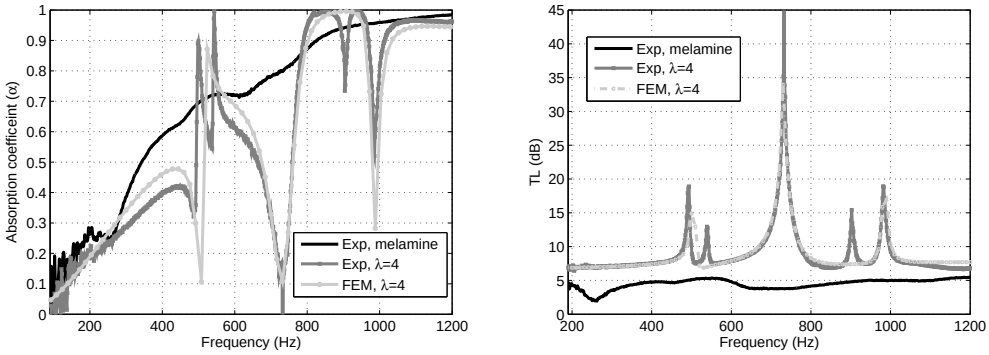

(a) (b)

Figure 9: Measurements and numerical results comparison of the membrane-cavity for λ=4 compared to the melamine foam: (a) Absorption coefficient and (b) Transmission loss.

are T_0=30.5 N/m for λ=3 and T_0=30 N/m for λ=4. Deviation between numerical and predicted values are observed, which is mainly due to the experimental errors resulting from the manual stretch process of the membrane. In the case of λ=3, three mean resonances are observed corresponding to one peak and two dips in the absorption curve (Fig.8 (a)) and three peaks for transmission loss (Fig.8 (b)), at respectively 395 Hz, 597 Hz and 760 Hz. In the case of λ=4, overall, resonances are shifted by approximately 30% (compared to λ=3 case) to 524 Hz, 722 Hz and 988 Hz. This confirms the ability of the membrane to control the resonance of the membrane-cavity system by varying the stretch ratio. The contribution to the sound absorbing efficiency of the porous material can be positive or negative at the membrane-cavity resonance frequencies. A similar approach based on the ASM analysis in section 4.1 is used in the present case, where an analysis of the normalized surface impedances is carried out. Thus, Fig.10 (a, b) shows the frequency evolution of the real (solid line) and imaginary (dashed line) parts of the normalized surface impedance resulting from experimental measurements for the membrane-cavity in foam Z_s^{MCRF} (for λ=3 and λ=4) embedded in the melamine foam compared to full foam reference configuration Z_s^{Mel}. Hence, above and below the resonance frequencies, the acoustic behavior of the assembly is quite similar to the one of the porous element. The imaginary part of the melamine foam impedance $\mathrm{Im}(Z_s^{\mathrm{Mel}})$ is important at low fre-

quency (Fig.10; dashed black line), demonstrating that the melamine foam behavior is mainly reactive due to the rigid backing condition. Moreover, the imaginary part reaches a null value for f=780 Hz inducing high absorption coefficient. For the latter frequency, the sample thickness corresponds approximately to half the wavelength.

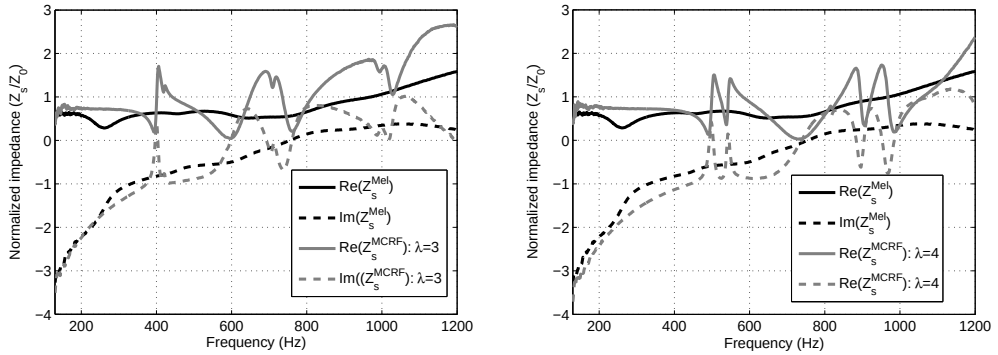

(a) (b)

Figure 10: Measured normalized surface impedance (Z_s/Z_0) of the membrane-cavity as function of frequency compared to the melamine foam: real part (solid line) and imaginary part (dashed lines) for (a) λ=3 and (b) λ=4.

For the membrane-cavity in foam (MCRF), peaks occur when the imaginary part $\mathrm{Im}(Z_s^{\mathrm{MCRF}})$ decreases to reach the null value and the real part $\mathrm{Re}(Z_s^{\mathrm{MCRF}})$ approaches the normalized surface impedance of the air ($\approx$1); an important impedance variation occurs and a high absorption coefficient is resulted at the resonance frequency as a consequence of a "short circuit", increasing thus the acoustic absorption of the MCRF assembly. Additionally, for the two successive resonances (dips in absorption and high amplitude peaks in transmission loss), the increase of $\mathrm{Im}(Z_s^{\mathrm{MCRF}})$ occurs in a frequency range where $\mathrm{Im}(Z_s^{\mathrm{Mel}})$ is fairly low as a result of the acoustic behavior of the porous material which is mainly resistive. The real part of the assembly is hence controlled by the porous material. A weak absorption is resulted due to the membrane resonances and the reduced area of the melamine (filling ratio).

The membrane-cavity in foam provides interesting resonances for frequencies above 400 Hz. Under the current design, the membrane with a stretch ratio

λ=3 can enhance the effective resonator absorption (only for the first resonance at 395 Hz) and the transmission loss at 395 Hz and 760 Hz. With a higher stretch ratio i.e, λ=4, frequencies can be increased to 524 Hz and 960 Hz respectively.

To investigate the effect of damping on the acoustic performances (peaks and dips) of the membrane-cavity in foam, numerical simulations are conducted for the λ=3 case using the two loss factor values η=0.01 and η=0.05. The results for sound absorption and transmission loss are shown in Fig.11.

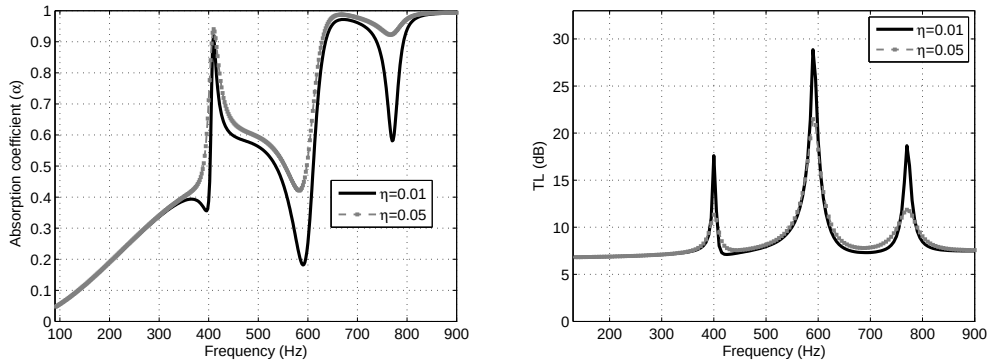

(a) (b)

Figure 11: Comparison of the numerical absorption coefficient (a) and transmission loss (b) results of the membrane-cavity in foam for two damping loss factor values η=0.01 and η=0.05.

A significant enhancement of the absorption is obtained when the loss factor increases from η=0.01 to η=0.05. Thus, all resonances amplitudes are decreasing to higher absorption coefficient values (first resonance by 0.02, the second by 0.25 and the third by 0.3), as shown in Fig.11 (a). However, a decline in the transmission performances of the device is resulted (Fig.11 (b)). Hence, lower peaks amplitudes are observed (first resonance by 5 dB, the second and the third by 7 dB). The obtained results show the high influence of the material damping on the design of these acoustic membraned systems. An experimental study of VHB membrane's damping effect on the acoustic performances of electroactive membraned Helmholtz resonators was carried out by Abbad et *al.* [42]. The results confirm the high contribution of the

stretch ratio on the membrane loss factor value and so on the absorption coefficient amplitude. The membrane material must be chosen in such a way as to obtain the best acoustic performances: reduced loss factor for the transmission and high loss factor for absorption.

4.3. Membrane-cavity HR in foam

A HR embedded in a melamine foam with its front wall made of an acrylic membrane (MCHRF) is now considered (Fig.1 (c)). Its acoustic behavior (for λ=3 and λ=4) is experimentally (dashed black line) and numerically (dashed gray line) compared to the full melamine foam (solid black line) in Fig.12. In the case of λ=3, two principal resonances are observed, one peak at f=187 Hz and one dip at f=675 Hz in the case of absorption (Fig.12 (a)). The same phenomenon is observed in the case of λ=4 (Fig.12 (b)). The first resonance is shifted by about 9 Hz to f=196 Hz compared to the one of λ=3, the second resonance is also shifted to higher frequency by 139 Hz to f=814 Hz. It is clearly observed that the second resonance is more sensitive to the variation of the stretch parameter λ. The stretched membrane replacing the rigid face of the HR leads to lower the first resonance frequency (Fig.6) by 37% for λ=3 and 52% for λ=4. This can be explained by considering works of Photiadis [43] dealing with a simple model of a spherical elastic shell HR and concluding that the dominant forces on the cavity walls are due to a buildup of pressure inside the enclosure which was equivalent to consider that the motion of most interest is the breathing mode. Norris [22] analyzed the elasticity effect of a spherical (and cylindrical) elastic HR based on a thin shell theory. Both authors concluded that the resonance shift phenomenon can be explained by the contribution of the elastic wall compliance. Thus, the effective compliance which decreases and the effective inertia which increases (compared to their standard forms for rigid HR) are modified by the elasticity parameter R_0=$(Z_s/Z_t)^{1/2}$ (Z_s being the effective total shell impedance and Z_t the total impedance to breathing motion of the shell). This analysis is still valid in the present study; the shift of the resonance is also due to the changes in the membrane-cavity HR compliance. Moreover, the membrane stiffness that counteract the motion of the fluid through the hole tends to decrease the resonator mass. The membrane is contracted due to the inertial force resulted from the pressure decrease in the cavity and from the exciting flow. By further analyzing the absorption coefficient curves, it can be said that at resonances, the energy is not transmitted but rather reflected. Below the resonance, the membrane behaves as a rigid wall, however, for frequen-

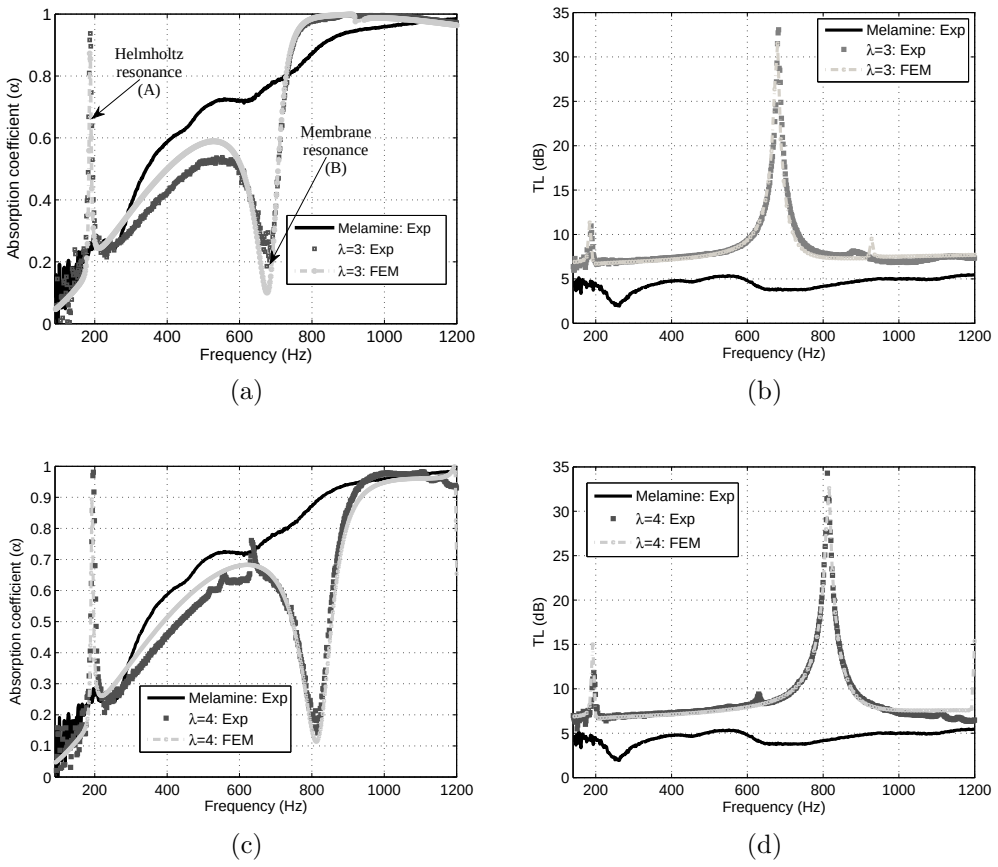

Figure 12: Experimental and numerical absorption coefficient and transmission loss at normal incidence of the membrane-cavity HR in foam compared to the experimental melamine foam result: a) Snapshot of the sound pressure field for λ=3 (maximum value inside the resonator) at the two resonances; b, d) Absorption coefficients for λ=3 and 4; c, e) TL for λ=3 and 4.

cies higher than its resonances, most of the energy would propagate through it enabling a high absorption (perfect absorption in the case of λ=4) due to the coupling with the cavity. Indeed, in addition to the contribution of the membrane stretch ratio λ, the dimensions and weight of the centrally placed mass play a preponderant role in the dynamic behavior of the membrane [44], mainly of the second resonance. The latter is attributed to the first annular-type mode (corresponding to the fourth mode shape of the membrane+neck system) where the added mass is nearly at rest and only the free membrane surface vibrates [45].
For λ=3 transmission loss curve (Fig.12 (c)), a peak of 11 dB amplitude but relatively narrow band is observed at the first resonance frequency. The same observations can be made for the λ=4 case (Fig.12 (d)) where the first resonance peak is 3 dB higher with 14 dB amplitude.
For the second resonance, the membrane present too much losses leading to a large attenuation in transmission and a poor absorption (because of the low reactance of the host foam). Here again, the integration of the membrane-cavity HR has a positive effect on the sound transmission loss of the melamine thanks to the added mass. The two resonances also affect and improve the sound transmission loss efficiency with a 34 dB amplitude for both λ=3 and 4 cases as shown in Fig.12 (c, d).

As in the previous case of membrane-cavity in foam, numerical simulations dealing with the HR membrane damping variation effect (η=0.01 and η=0.05) are performed for the λ=3 case. Results for sound absorption and transmission loss are shown in Fig.13.

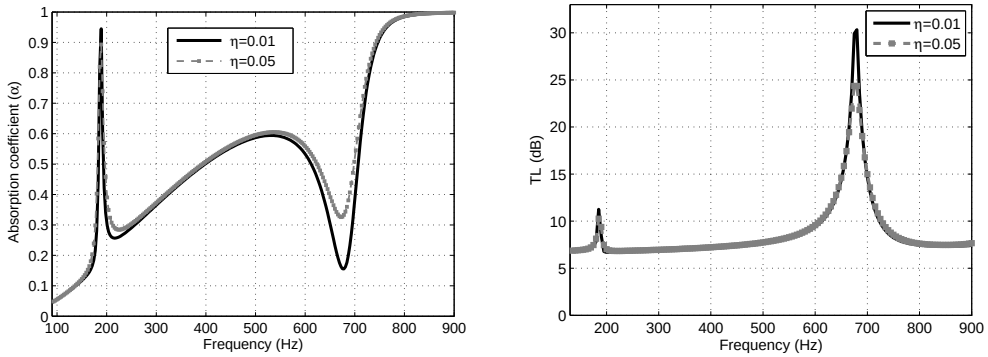

(a) (b)

Figure 13: Comparison of the numerical absorption coefficient (a), and transmission loss (b) results of the membrane-cavity HR for two damping loss factor values η=0.01 and η=0.05.

As observed from Fig.13 (a), the increase of the loss factor η contributes to the variation of the absorption coefficient. The first (Helmholtz resonance) is decreased (by 0.05 amplitude) when the loss factor increases from 0.01 to 0.05, which reduces the performances of the device, however, this contributes positively to the second resonance (membrane resonance) which increases (by 0.15 amplitude), improving therefore the acoustic absorption coefficient in higher frequencies. In the case of transmission loss (Fig.13 (b)), the first (by 1 dB) and the second (by 5.5 dB) resonances are reduced when the loss factor is increased. Hence, a decline in the transmission performances of the device is resulted. The obtained results show the importance of the material damping on the design of these acoustic membraned systems.
Under the current system parameters, the membrane of λ=3 and 4 can tune the effective membrane-cavity HR absorption and transmission loss at two specific resonances resulting from the interactions between the membrane vibrations, its stiffness change resulted from the variation of the parameter λ and the cavity dimension. On the other hand, the membrane damping plays a crucial role in acoustic performances of the proposed devices.
The membrane-cavity HR configurations for λ=3 and λ=4 have similar global acoustic behavior. One peak and one dip in the case of absorption (Fig.12 (a, b)) and two peaks in sound transmission loss (Fig.12 (c, d)). The frequency evolution of the real and imaginary parts of the normalized surface impedance

Z_s^{MCHRF} (Fig.14 (a, b)) are assessed. Peaks occur when $\mathrm{Im}(Z_s^{\mathrm{MCHRF}})$ reaches a null value and at the same time $\mathrm{Re}(Z_s^{\mathrm{MCHRF}})$ becomes almost equal to the air impedance ($\approx$1), an important impedance variation occurs and a high absorption coefficient is resulted thanks to the Helmholtz type resonance. The analysis of the negative absorption can be accomplished following the observations made in Section 4.1. The increase of $\mathrm{Im}(Z_s^{\mathrm{MCHRF}})$ occurs in a frequency range where $\mathrm{Im}(Z_s^{\mathrm{Mel}})$ is fairly low as a result of the resistive behavior of the porous material. Hence, a weak absorption is resulted because of the drop of $\mathrm{Re}(Z_s^{\mathrm{MCHRF}})$ due to the membrane resonance, the low absorption surface of the foam and the resonator filling ratio. Also, high amplitude peaks in sound transmission loss is resulted.

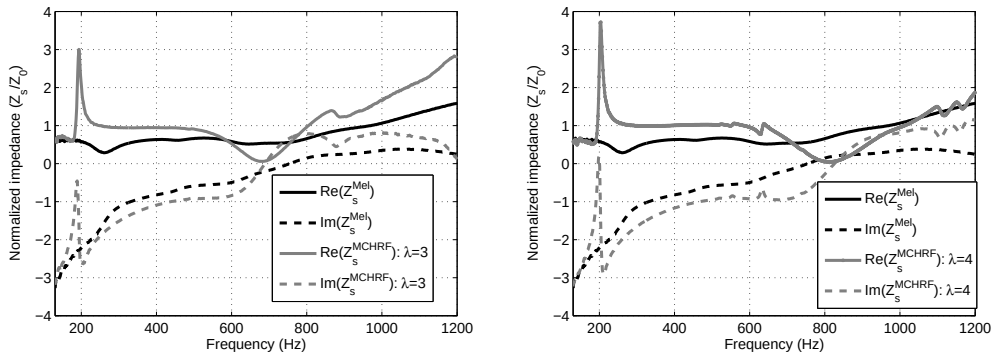

(a) (b)

Figure 14: Measured normalized surface impedance (Z_s/Z_0) of the membrane-cavity Helmholtz resonator in foam (MCHRF) as function of frequency compared to the melamine foam: real part (solid line) and imaginary part (dashed lines) for (a) λ=3 and (b) λ=4.

5. Conclusion

The design of efficient acoustic devices in the low frequency regime is strongly desired. In this work, the acoustic properties of a soft acrylic membrane-cavity with two stretch ratios λ=3 and 4 embedded in a melamine foam have been numerically and experimentally investigated. Under the chosen system parameters, enhancement in the sound absorption coefficient (Helmholtz resonance) and sound transmission loss are obtained for frequencies above 400 Hz. By addition of a neck to the cavity, a front membrane-cavity Helmholtz resonator is obtained. The device allows high single sound

absorption (at Helmholtz resonance) in low frequencies and two transmission loss peaks. However, the resonator may contribute negatively to the sound absorbing efficiency and this decrease is shown to depend on the membrane resonance frequency. The negative effect is transformed into an interesting contribution for the sound transmission loss which becomes very large at medium and high frequencies. The resonance phenomenon can be illustrated by considering the interactions between the membrane vibrations, its stiffness change resulted from the variation of the membrane stretch ratio λ and the geometry of the Helmholtz cavity. Since the addition of the membrane to the system may degrade the absorption behavior, a transmission configuration is therefore preferred as future application. The presented numerical model is able to represent fairly well the vibro-acoustical phenomena occurring in the studied systems under plane wave propagation assumptions. However, the membrane manufacturing process must be carried out meticulously in order to reduce its in plane force uncertainties and hence, overcome the identification process. Precise knowledge of the mounting conditions and membrane losses are required for the design of optimal configurations allowing perfect absorption and/or transmission loss enhancement. As well, the high sensitivity of the membrane in-plane force response can be used as part of adaptive systems. Indeed, these membranes can be used as electroactive devices, allowing the control of the applied voltage, to tune the membrane in-plane force and then the characteristic frequencies of the resonators.

Acknowledgments

The authors would like to thank the National Sciences and Engineering Research Council of Canada (NSERC) and CRIAQ (Consortium de recherche et d'innovation en aérospatiale au Québec) for providing financial support. This work has been performed in cooperation with the EUR EIPHI program (ANR-17-EURE-0002).

Appendix A. Behavior description of hyperelastic materials

Large strain elastic (or hyperelastic) materials are characterized through an energy potential, which describes the strain energy as a function of the deformation. The total strain energy density W_s is defined as [46]

$$W_s = W_{iso} + W_{vol}, \tag{A.1}$$

where W_{iso} is the isochoric strain energy density and W_{vol} is the volumetric strain energy density.
The second Piola-Kirchhoff stress tensor is given by

$$S = -p_p J_v C^{-1} + 2\frac{\partial W_{iso}}{\partial C}, \tag{A.2}$$

where p_p is the volumetric stress (pressure), J_v is the volume ratio, and C is the right Cauchy-Green tensor.
Classical hyperelastic models assume near incompressibility and thus the volumetric terms are dropped [47]. The first component of the first Piola-Kirchhoff stress tensor P_1 and the Cauchy stress tensor σ, can be expressed as a function of the second Piola-Kirchhoff stress tensor S_1 as

$$P_1 = FS_1, \tag{A.3}$$

and

$$\sigma = J_v^{-1} F S_1 F^T, \tag{A.4}$$

F being the deformation gradient.
The strain energy density W_s is expressed in terms of principal stretches λ_1, λ_2 and λ_3. In the case of a uniaxial test (1D), incompressibility requires: $\lambda_1 = \lambda$ and $\lambda_2 = \lambda_3 = \frac{1}{\lambda}$ (λ being defined as $\lambda = \frac{L}{L_0}$ (where L is the deformed length of the characterized specimen and L_0 its original length).
The normal component of the second Piolla-Kirchoff tensor S_1 is expressed as function of λ:

$$S_1 = 2(\frac{1}{\lambda} - \frac{1}{\lambda^4})(\lambda\frac{\partial W_{iso}}{\partial I_1} + \frac{\partial W_{iso}}{\partial I_2}). \tag{A.5}$$

I_1 and I_2 are isochoric invariants and are given by

$$I_1 = \lambda^2 + \frac{2}{\lambda}, \tag{A.6}$$

and

$$I_2 = 2\lambda + \frac{1}{\lambda^2}. \tag{A.7}$$

In the case of uniaxial test, the first component of the Piola-Kirchhoff stress tensor P_1 is given by

$$P_1 = \frac{F_r}{A_0} = \lambda S_1, \tag{A.8}$$

and the first Cauchy stress tensor

$$\sigma_1 = \lambda^2 S_1. \tag{A.9}$$

A_0 is the original cross-section area of the test specimen and F_r is the applied force.

References

[1] J. F. Allard, N. Atalla, Propagation of Sound in Porous Media, John Wiley & Sons, Ltd, 2009. doi:10.1002/9780470747339.
URL https://doi.org/10.1002%2F9780470747339

[2] V. Romero-García, G. Theocharis, O. Richoux, V. Pagneux, Use of complex frequency plane to design broadband and sub-wavelength absorbers, The Journal of the Acoustical Society of America 139 (6) (2016) 3395–3403. doi:10.1121/1.4950708.
URL https://doi.org/10.1121%2F1.4950708

[3] N. Jiménez, W. Huang, V. Romero-García, V. Pagneux, J.-P. Groby, Ultra-thin metamaterial for perfect and quasi-omnidirectional sound absorption, Applied Physics Letters 109 (12) (2016) 121902. doi:10.1063/1.4962328.
URL https://doi.org/10.1063%2F1.4962328

[4] U. Ingård, S. Labate, Acoustic circulation effects and the nonlinear impedance of orifices, The Journal of the Acoustical Society of America 22 (2) (1950) 211–218. doi:10.1121/1.1906591.
URL https://doi.org/10.1121%2F1.1906591

[5] U. Ingard, On the theory and design of acoustic resonators, The Journal of the acoustical society of America 25 (6) (1953) 1037–1061.

[6] I. Lee, A. Selamet, K. V. Tallio, Helmholtz resonator with an extended neck, The Journal of the Acoustical Society of America 110 (5) (2001) 2671–2671. doi:10.1121/1.4809009.
URL https://doi.org/10.1121%2F1.4809009

[7] J. Hsu, K. Ahuja, Cavity noise control using helmholtz resonators, in: Aeroacoustics Conference, American Institute of Aeronautics and Astronautics, 1996. doi:10.2514/6.1996-1675.
URL https://doi.org/10.2514%2F6.1996-1675

[8] P. Tang, W. Sirignano, Theory of a generalized helmholtz resonator, Journal of Sound and Vibration 26 (2) (1973) 247–262. doi:10.1016/s0022-460x(73)80234-2.
URL https://doi.org/10.1016%2Fs0022-460x%2873%2980234-2

[9] R. A. Prydz, L. S. Wirt, H. L. Kuntz, L. D. Pope, Transmission loss of a multilayer panel with internal tuned helmholtz resonators, The Journal of the Acoustical Society of America 87 (4) (1990) 1597–1602. doi:10.1121/1.399407.
URL https://doi.org/10.1121%2F1.399407

[10] H. L. Kuntz, R. A. Prydz, F. J. Balena, R. J. Gatineau, Development and testing of cabin sidewall acoustic resonators for the reduction of cabin tone levels in propfan-powered aircraft, Noise Control Engineering Journal 37 (3) (1991) 129. doi:10.3397/1.2827801.
URL https://doi.org/10.3397%2F1.2827801

[11] I. U. Borchers, Acoustic protection on payload fairings of expendable launch vehicles, The Journal of the Acoustical Society of America 103 (5) (1998) 2259. doi:10.1121/1.422707.
URL https://doi.org/10.1121%2F1.422707

[12] S. Sugie, J. Yoshimura, T. Iwase, Effect of inserting a helmholtz resonator on sound insulation in a double-leaf partition cavity, Acoustical Science and Technology 30 (5) (2009) 317–326. doi:10.1250/ast.30.317.
URL https://doi.org/10.1250%2Fast.30.317

[13] A. I. Komkin, M. A. Mironov, A. I. Bykov, Sound absorption by a helmholtz resonator, Acoustical Physics 63 (4) (2017) 385–392. doi:10.1134/s1063771017030071.
URL https://doi.org/10.1134%2Fs1063771017030071

[14] C.-L. Ding, X.-P. Zhao, Multi-band and broadband acoustic metamaterial with resonant structures, Journal of Physics D: Applied Physics 44 (21) (2011) 215402. doi:10.1088/0022-3727/44/21/215402.
URL https://doi.org/10.1088%2F0022-3727%2F44%2F21%2F215402

[15] C. Lagarrigue, J. P. Groby, V. Tournat, O. Dazel, O. Umnova, Absorption of sound by porous layers with embedded periodic arrays of resonant inclusions, The Journal of the Acoustical Society of America 134 (6) (2013) 4670–4680. doi:10.1121/1.4824843.
URL https://doi.org/10.1121%2F1.4824843

[16] C. Boutin, Acoustics of porous media with inner resonators, The Journal of the Acoustical Society of America 134 (6) (2013) 4717–4729. doi:10.1121/1.4824965.
URL https://doi.org/10.1121%2F1.4824965

[17] J.-P. Groby, C. Lagarrigue, B. Brouard, O. Dazel, V. Tournat, B. Nennig, Enhancing the absorption properties of acoustic porous plates by periodically embedding helmholtz resonators, The Journal of the Acoustical Society of America 137 (1) (2015) 273–280.

[18] O. Doutres, N. Atalla, H. Osman, Transfer matrix modeling and experimental validation of cellular porous material with resonant inclusions, The Journal of the Acoustical Society of America 137 (6) (2015) 3502–3513. doi:10.1121/1.4921027.
URL https://doi.org/10.1121%2F1.4921027

[19] C. J. Naify, C.-M. Chang, G. McKnight, S. Nutt, Transmission loss and dynamic response of membrane-type locally resonant acoustic metamaterials, Journal of Applied Physics 108 (11) (2010) 114905. doi:10.1063/1.3514082.
URL https://doi.org/10.1063%2F1.3514082

[20] Z. Yang, J. Mei, M. Yang, N. H. Chan, P. Sheng, Membrane-type acoustic metamaterial with negative dynamic mass, Physical Review Letters 101 (20). doi:10.1103/physrevlett.101.204301.
URL https://doi.org/10.1103%2Fphysrevlett.101.204301

[21] T.-Y. Huang, C. Shen, Y. Jing, Membrane- and plate-type acoustic metamaterials, The Journal of the Acoustical Society of America 139 (6) (2016) 3240–3250. doi:10.1121/1.4950751.
URL https://doi.org/10.1121%2F1.4950751

[22] A. N. Norris, G. Wickham, Elastic helmholtz resonators, The Journal of the Acoustical Society of America 93 (2) (1993) 617–630. doi:10.1121/1.405481.
URL https://doi.org/10.1121%2F1.405481

[23] S. Griffiths, B. Nennig, S. Job, Porogranular materials composed of elastic helmholtz resonators for acoustic wave absorption, The Journal of the Acoustical Society of America 141 (1) (2017) 254–264. doi:

10.1121/1.4973691.
URL https://doi.org/10.1121%2F1.4973691

[24] Z. Lu, H. Godaba, Y. Cui, C. C. Foo, M. Debiasi, J. Zhu, An electronically tunable duct silencer using dielectric elastomer actuators, The Journal of the Acoustical Society of America 138 (3) (2015) EL236–EL241. doi:10.1121/1.4929629.
URL https://doi.org/10.1121%2F1.4929629

[25] X. Yu, Z. Lu, L. Cheng, F. Cui, Vibroacoustic modeling of an acoustic resonator tuned by dielectric elastomer membrane with voltage control, Journal of Sound and Vibration 387 (2017) 114–126. doi:10.1016/j.jsv.2016.10.022.
URL https://doi.org/10.1016%2Fj.jsv.2016.10.022

[26] R. Venegas, C. Boutin, Acoustics of permeo-elastic materials, Journal of Fluid Mechanics 828 (2017) 135–174. doi:10.1017/jfm.2017.505.
URL https://doi.org/10.1017%2Fjfm.2017.505

[27] Y. Champoux, J.-F. Allard, Dynamic tortuosity and bulk modulus in air-saturated porous media, Journal of Applied Physics 70 (4) (1991) 1975–1979. doi:10.1063/1.349482.
URL https://doi.org/10.1063%2F1.349482

[28] R. Kirby, A. Cummings, Prediction of the bulk acoustic properties of fibrous materials at low frequencies1a shorter version of this paper was presented at the EuroNoise conference, lyon, france, 21-23 march 19951, Applied Acoustics 56 (2) (1999) 101–125. doi:10.1016/s0003-682x(98)00015-2.
URL https://doi.org/10.1016%2Fs0003-682x%2898%2900015-2

[29] P. A. L. S. Martins, R. M. N. Jorge, A. J. M. Ferreira, A comparative study of several material models for prediction of hyperelastic properties: Application to silicone-rubber and soft tissues, Strain 42 (3) (2006) 135–147. doi:10.1111/j.1475-1305.2006.00257.x.
URL https://doi.org/10.1111%2Fj.1475-1305.2006.00257.x

[30] M. Mooney, A theory of large elastic deformation, Journal of Applied Physics 11 (9) (1940) 582–592. doi:10.1063/1.1712836.
URL https://doi.org/10.1063%2F1.1712836

[31] R. W. Ogden, Large deformation isotropic elasticity—on the correlation of theory and experiment for incompressible rubberlike solids, Rubber Chemistry and Technology 46 (2) (1973) 398–416. doi:10.5254/1.3542910.
URL https://doi.org/10.5254%2F1.3542910

[32] O. Doutres, N. Atalla, Acoustic contributions of a sound absorbing blanket placed in a double panel structure: Absorption versus transmission, The Journal of the Acoustical Society of America 128 (2) (2010) 664–671. doi:10.1121/1.3458845.
URL https://doi.org/10.1121%2F1.3458845

[33] C. Zwikker, C. Kosten, Sound Absorbing Materials, Elsevier Publishing Company, 1949.
URL https://books.google.fr/books?id=ezUOnQEACAAJ

[34] Y. Salissou, R. Panneton, O. Doutres, Complement to standard method for measuring normal incidence sound transmission loss with three microphones, The Journal of the Acoustical Society of America 131 (3) (2012) EL216–EL222. doi:10.1121/1.3681016.
URL https://doi.org/10.1121%2F1.3681016

[35] 3M Industrial Adhesives and Tapes Division, 3M VHB Tape Specialty Tapes (2015).

[36] C. M. Roland, M. MUNJAL, Formulas of acoustics, Springer Science & Business Media, 2004. doi:10.1007/978-3-662-07296-7.
URL https://doi.org/10.1007/978-3-662-07296-7

[37] N. Jiménez, T. J. Cox, V. Romero-García, J.-P. Groby, Metadiffusers: Deep-subwavelength sound diffusers, Scientific Reports 7 (1). doi:10.1038/s41598-017-05710-5.
URL https://doi.org/10.1038%2Fs41598-017-05710-5

[38] M. R. Stinson, The propagation of plane sound waves in narrow and wide circular tubes, and generalization to uniform tubes of arbitrary cross-sectional shape, The Journal of the Acoustical Society of America 89 (2) (1991) 550–558. doi:10.1121/1.400379.
URL https://doi.org/10.1121%2F1.400379

[39] J. Y. Chung, D. A. Blaser, Transfer function method of measuring induct acoustic properties. II. experiment, The Journal of the Acoustical Society of America 68 (3) (1980) 914–921. doi:10.1121/1.384779.
URL https://doi.org/10.1121%2F1.384779

[40] M. Reynolds, S. Daley, An active viscoelastic metamaterial for isolation applications, Smart Materials and Structures 23 (4) (2014) 045030. doi:10.1088/0964-1726/23/4/045030.
URL https://doi.org/10.1088%2F0964-1726%2F23%2F4%2F045030

[41] B. Brouard, Validation par holographie acoustique de nouveaux modèles pour la propagation des ondes dans les matériaux poreux stratifiés (acoustic holographic validation of new models for wave propagation in stratified porous materials), Ph.D. thesis (1994).

[42] A. Abbad, K. Rabenorosoa, M. Ouisse, N. Atalla, Adaptive helmholtz resonator based on electroactive polymers: modeling, characterization, and control, Smart Materials and Structures 27 (10) (2018) 105029. doi:10.1088/1361-665x/aad939.
URL https://doi.org/10.1088%2F1361-665x%2Faad939

[43] D. M. Photiadis, The effect of wall elasticity on the properties of a helmholtz resonator, The Journal of the Acoustical Society of America 90 (2) (1991) 1188–1190. doi:10.1121/1.402026.
URL https://doi.org/10.1121%2F1.402026

[44] Z. Liu, Locally resonant sonic materials, Science 289 (5485) (2000) 1734–1736. doi:10.1126/science.289.5485.1734.
URL https://doi.org/10.1126%2Fscience.289.5485.1734

[45] F. Langfeldt, W. Gleine, O. von Estorff, An efficient analytical model for baffled, multi-celled membrane-type acoustic metamaterial panels, Journal of Sound and Vibration 417 (2018) 359–375. doi:10.1016/j.jsv.2017.12.018.
URL https://doi.org/10.1016%2Fj.jsv.2017.12.018

[46] C. M. Roland, Viscoelastic Behavior of Rubbery Materials, Oxford University Press, 2011. doi:10.1093/acprof:oso/9780199571574.001.0001.

URL https://doi.org/10.1093%2Facprof%3Aoso%2F9780199571574.001.0001

[47] A. Ibrahimbegovic, Nonlinear Solid Mechanics, Springer Netherlands, 2009. doi:10.1007/978-90-481-2331-5.
URL https://doi.org/10.1007%2F978-90-481-2331-5